Applied Surface Science 462 (2018) 1008–1016

Contents lists available at ScienceDirect

Applied Surface Science

journal homepage: www.elsevier.com/locate/apsusc

Full Length Article

Selective atomic layer deposition of $MoSi_x$ on Si (0 0 1) in preference to silicon nitride and silicon oxide

Jong Youn Choi[a], Christopher F. Ahles[a], Raymond Hung[c], Namsung Kim[c], Andrew C. Kummel[b,*]

[a] *Materials Science and Engineering Program, University of California, San Diego, La Jolla, CA 92093, United States*
[b] *Department of Chemistry Biochemistry, University of California, San Diego, La Jolla, CA 92093, United States*
[c] *Applied Materials, Inc, Santa Clara, CA 95054, United States*

ARTICLE INFO

Keywords:
Atomic layer deposition
Area-selective deposition
Molybdenum Silicide ($MoSi_2$)

ABSTRACT

Highly selective deposition of $MoSi_x$ on Si in preference to SiO_2 and SiN_x was achieved via atomic layer deposition (ALD) using MoF_6 and Si_2H_6 at 120 °C. The selectivity was enabled by the lack of chemical reactivity between the reactants and the SiO_2 and SiN_x substrates. In contrast, MoF_6 nucleated in a self-limiting manner on H-terminated Si, and a following Si_2H_6 exposure reduced MoF_x to Mo^0 which is consistent with Mo-Si bond formation. X-Ray photoelectron spectroscopy (XPS) revealed that the 5 ALD cycles of MoF_6 and Si_2H_6 selectively deposited a substoichiometric $MoSi_2$ film on the Si substrate in contrast to previous results showing a nearly pure Mo deposition. Extra Si_2H_6 doses on the substoichiometric $MoSi_2$ film incorporated more Si into the film without disturbing the inherent selectivity over SiO_2 and SiN_x. A depth-profiling study showed that the bulk of the film has $Si/Mo = 1.7–1.9$ with $< 10\%$ F and O impurities. The data is consistent with higher pressure Si_2H_6 doses inducing silicide formation instead of metal deposition. To verify selectivity on the nanoscale, the selective deposition of $MoSi_x$ was investigated on a patterned Si wafer containing three-dimensional (3D) nanoscale SiO_2 and SiN_x features. Cross-sectional transmission electron microscopy (TEM) showed that selective $MoSi_x$ deposition was achieved on nanoscale 3D structures. AFM documented that there were less than 10 nuclei/μm^2 on SiO_2.; since SiO_2 has $\sim 10^6/\mu m^2$ OH groups, this corresponds to an intrinsic selectivity of about 10^6:1 between the OH groups on SiO_2 and Si-H groups on Si. This inherent substrate-dependent selectivity for silicide deposition allows the elimination of pre-positioning of passivants.

1. Introduction

Exact positioning of materials on nanoscale devices is required to manipulate atomic-scale properties for next-generation nanoelectronics [1–3]. For semiconductor fabrication, detailed positioning of materials with excellent conformality and stoichiometry is required to meet the demand for cost, yield, and throughput [4]. As metal-oxidesemiconductor field effect transistors (MOSFETs) are scaled to less than < 10 nm channel length, there is a need to overcome the constraints originating from top-down processes such as damage from reactive ion etching and structural complexity in alignments on three-dimension (3D) surfaces [3–6].

Recently, as MOSFET devices have been fabricated in 3D structures (FinFETs), there has been increasing interest in area-selective deposition on the nanoscale while maintaining conformal film quality since area-selective atomic layer deposition (ALD) eliminates patterning steps and complexity particular to 3D devices such as lithography onto 3D structures [6]. It has been demonstrated that selective ALD can be accomplished using self-assembled monolayers (SAMs) as passivation layers [7–9]. The passivation layers block or eliminate surface functional groups that are reactive towards ALD precursors so that selectivity can be obtained; however, this necessitates the selective deposition of the passivation layer. Furthermore, often the passivation layers must be selectively removed after the selective deposition [10]. Therefore, an alternative method to obtain selectivity has been suggested which is to utilize substrate-dependent reactivity of ALD precursors [11–14]. Kalayan et al. [14] reported the intrinsic substrate-dependent selectivity of W metal deposition on Si over SiO_2 using WF_6 and SiH_4. The inherent substrate selectivity was ascribed to only H-terminated Si readily being reactive to WF_6(g) to form SiF_4(g) products since Si-O bonds are stable enough not to be attacked by WF_6 [13,24]. Kalayan et al. suggested that by adding a H_2 carrier gas with WF_6 during the deposition process, the selectivity window (number of ALD cycles over which selectivity is retained) could be improved. It was hypothesized that the ALD by-product HF passivated

---

* Corresponding author.
E-mail address: akummel@ucsd.edu (A.C. Kummel).

https://doi.org/10.1016/j.apsusc.2018.08.072
Received 16 May 2018; Received in revised form 26 July 2018; Accepted 6 August 2018

the –OH nucleation sites on SiO_2 in the form of SiO_xF_y which is not reactive towards WF_6.

Transition metal disilicides such as $TiSi_2$, $CoSi_2$ and $MoSi_2$ are capable of reducing the electrical resistance at the contact regions and tuning the contact work function in MOSFETs [15,16]. It is important to reduce the parasitic resistance since the performance of scaled devices with < 10 nm channel length can be strongly affected by parasitic resistance. The conventional methods to form silicides involve a high temperature anneal after metal deposition onto Si or by direct deposition of silicides using evaporation or co-sputtering [17]. These methods readily form silicides of the desired stoichiometry, but they may not be applicable to complicated 3D structures due to the Si consumption, poor step coverage, and insufficient thickness control for scaled devices. There have been several studies on W or Mo metal ALD using WF_6 or MoF_6 and SiH_4 or Si_2H_6, but little is documented on ALD of silicide [14,18]. Bernal-Ramos et al. carried out $CoSi_2$ ALD on H-terminated Si (1 1 1) at 140 °C using an organometallic Co precursor (^{t}Bu-AllylCo(CO)$_3$) and trisilane (Si_3H_8) [19]. NbSi deposition was achieved by Proslier et al. using NbF_5 and Si_2H_6 at a deposition temperature of 150–400 °C [20]. Using MoF_6 and Si_2H_6 as the reactants, Seghete et al. studied the nucleation and growth characteristics of Mo metal ALD between 90 and 150 °C using a quartz crystal microbalance [18]. It was hypothesized that Si_2H_6 acts as a sacrificial reducing agent for MoF_6 and leaves reduced Mo metal as a final product which was previously suggested in W metal ALD or CVD using WF_6 and SiH_4 [14,28]. While the inherent selectivity of metal deposition on Si over thermally grown pristine SiO_2 was previously reported using MoF_6 or WF_6, in 3D architectures (FinFETs), selective silicide growth on Si over SiO_2 as well as SiN_x or SiON which are ion damaged is also required. Selective silicide deposition on Si over ion damaged SiN_x or SiON is a critical challenge in 3D nanostructures.

The objective of the present study is to quantify on the nanoscale the selective deposition of $MoSi_x$ on Si in preference to SiO_2, SiON and SiN_x using the inherent substrate selectivity of MoF_6 and Si_2H_6. The selectivity on planar samples was quantified with X-ray photoelectron spectroscopy (XPS) as well as atomic force microscopy (AFM) in order to count the number of unwanted nuclei on SiO_2, while the selectivity on 3D nanoscale structures was probed by both XPS and transition electron microscopy (TEM). To achieve stoichiometric $MoSi_2$, additional Si insertion after the ALD cycles was performed by dosing Si_2H_6 onto the Mo rich $MoSi_x$ film. The resistivity of the $MoSi_x$ film was obtained by using 4-probe electrical measurements.

2. Experimental

Four types of samples were employed: P-type Si (1 0 0) (Boron-doped, Virginia Semiconductor), thermally grown SiO_2 on Si (1 0 0) (University Wafer), SiON (Applied Materials) and patterned samples having Si, SiO_2 and SiN_x. The SiON in this study is Si_3N_4 which has been subjected to reactive ion etching and plasma ashing in oxygen during fabrication, and therefore contains oxygen; this mimics the conditions of Si_3N_4 after processing in integrated 3D nanoscale devices. The samples were diced into 12 mm × 3 mm pieces and degreased with acetone, methanol and deionized (DI) H_2O. The native oxide on Si was removed by immersing the degreased samples into a 0.5% HF(aq) solution for 30 s. For consistency in cleaning procedure, the SiO_2, SiON and patterned samples were subjected to the same cleaning procedure. The samples were blow-dried using high purity N_2 gas. Two or three samples out of the Si, SiO_2, SiON and patterned sample were loaded together on a single sample holder to expose the samples to the same ALD conditions. The samples were loaded into a load lock chamber pumped by a turbo molecular pump and backed by a mechanical pump. The base pressure of the load lock was $\sim 2.0 \times 10^{-7}$ Torr. Subsequently, the samples were transferred in-situ to an ultra-high vacuum chamber with a base pressure of $\sim 3.0 \times 10^{-10}$ Torr pumped by an ion pump and titanium sublimation pump. The ultra-high vacuum chamber was equipped with a monochromatic XPS (XM 1000 MkII/SPHERA, Omicron Nanotechnology), STM (Omicron Nanotechnology) and annealing system using a pyrolytic boron nitride (PBN) heater.

The samples were first annealed at 120 °C in the ultra-high vacuum chamber and the chemical composition of the samples were determined using XPS. Afterwards, the samples were transferred in-situ to a home-made reaction chamber having a base pressure of $\sim 5.0 \times 10^{-7}$ Torr. For $MoSi_x$ deposition, MoF_6 (Synquest Laboratories, 99%) and Si_2H_6 (Air Liquide, 99.99%) precursors were employed.

During the ALD cycles, a constant purge of N_2 (80 mTorr) was used, and the pressure of this purge was controlled using a leak valve. The MoF_6 and Si_2H_6 doses were regulated using pneumatic valves controlled by a LabView program. An expansion volume was employed for the MoF_6 and Si_2H_6 doses. This consisted of filling a secondary volume with MoF_6 or Si_2H_6 and dosing the precursors from their respective secondary volumes. The fill/dose times for the MoF_6 were 40 ms/50 ms and for Si_2H_6 the fill/dose times were 18 ms/18 ms. The exposures of MoF_6 and Si_2H_6 were calculated in terms of Langmuirs (L) where 1 L = 1×10^{-6} Torr × 1 s. The pressure spikes during the exposures were monitored using a Convectron gauge in the reaction chamber. The doses were 1.8 MegaL for MoF_6 and 4.2 MegaL for Si_2H_6 with a 2-min wait time between the doses. The samples were heated using a pyrolytic boron nitride (PBN) heater, and the temperature was maintained at 120 °C. The chamber walls were maintained at 80 °C. After the deposition cycles, the samples were transferred in-situ to the ultra-high vacuum chamber for XPS and STM. For the XPS measurement, the X-rays were generated by an Al Kα anode (1486.7 eV). XPS data was acquired using constant analyzer-energy (CAE) with a step width of 0.1 eV and a pass energy of 50 eV. The XPS detector was at 60° to the sample normal (30° take-off angle from the sample surface) with a detector-acceptance angle of 7°. XPS spectra were analyzed after correcting each peak area with its respective relative sensitivity factor using a Casa XPS v.2.3 program. All of the chemical components in this work were normalized to the sum of all components. STM was performed with a sample bias of −1.8 V and a constant current of 200 pA.

To investigate the elemental composition of the bulk of the film, Ar^+ sputtering was performed in conjunction with XPS. A lens voltage of 5 kV with a beam current of 1.2 μA at 6.0×10^{-7} Torr of Ar was employed; since a raster was used to cover the full sample area, the current density was approximately 1.2 μA/50 mm^2. The $MoSi_x$ sample was maintained at 25 °C during sputtering to minimize any thermal desorption of SiH_xF_y or SiF_4 compounds from the surface.

3. Results and discussion

Fig. 1(a) shows the XPS chemical composition of the HF cleaned Si surface before and after sequential doses of MoF_6 and Si_2H_6 at 120 °C (note: the raw XPS spectra are presented in the supplement). After the HF clean, all the Si was in an oxidation state of 0 with 9% O and 12% C contamination which was most likely due to adventitious hydrocarbon adsorption during the sample transfer into vacuum. HF(aq) is known to eliminate native oxide on Si and leaves the Si surface H-terminated [21]. Note that the yellow bars (Si 2p) in Fig. 1 indicate the total amount of Si while the gray bars (Si (0)) indicate the amount of Si which is in an oxidation state of 0 (Si^0). The amount of Mo^0 (Mo (0), the purple bars) and the total amount of Mo (Mo 3d, the pink bars) were also plotted separately to emphasize the amount of pure $MoSi_x$. After the 5.4 MegaL of MoF_6 at 120 °C, 14% Mo and 38% F were deposited on the HF cleaned Si surface. After an additional 5.4 MegaL of MoF_6 at 120 °C were dosed, the Mo concentration increased from 14% to 16% and the F concentration increased from 38% to 42%. This small increase in Mo and F content after an additional 5.4 MegaL of MoF_6 shows that the reaction of MoF_6 on HF cleaned Si is self-limiting (also see Fig. S5). After the Si surface was saturated with MoF_x, the ratio of F/Mo was 2.6 and all of the Si was in an oxidation state of 0. Sequential doses of 4.2 MegaL of Si_2H_6 and 42 MegaL of Si_2H_6 indicate that the Si_2H_6 reaction also saturates on the MoF_x covered Si surface. It is shown below

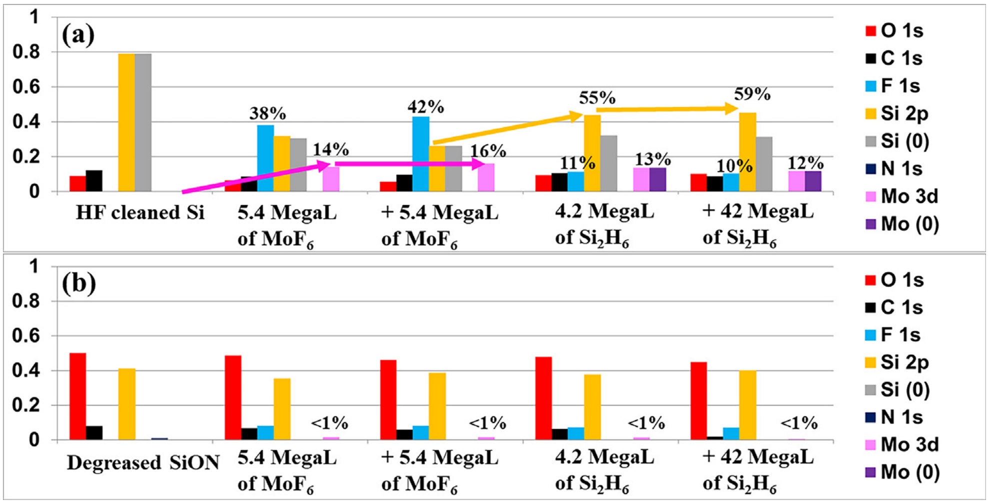

Fig. 1. XPS of $MoSi_x$ film selectively grown on HF cleaned Si versus degreased SiON after a cycle of saturating doses of MoF_6 and Si_2H_6. (a) 2 sets of 5.4 MegaL of MoF_6 were dosed on HF cleaned Si at 120 °C. XPS showed saturation of Mo at 16%. Afterward, 4.2 MegaL and an additional 42 MegaL of Si_2H_6 were dosed onto the MoF_6-saturated Si surface at 120 °C; Si was saturated at 59%. (b) The same amounts of MoF_6 and Si_2H_6 were dosed on the degreased SiON at 120 °C. Degreased SiON showed an inherent non-reactivity to both MoF_6 and Si_2H_6 and had < 1% Mo detected on the surface.

that with a thicker sub-stoichiometric $MoSi_2$ film, additional Si can be forced onto the surface. However, the Si_2H_6 reacts in a self-limiting manner on a thinner (monolayer) film of Mo. After saturation of Si_2H_6, the Si content was 59% and F decreased to 10%. Since the substrate is Si, this increase of the Si content after dosing Si_2H_6 could be partially ascribed to the substrate since F desorption occurred in the form of SiH_xF_y or SiF_4. However, attenuation of the Mo after Si_2H_6 dose was observed which is consistent with the deposition of Si. The deposition of Si was also demonstrated by previously published studies using WF_6 and Si_2H_6 or MoF_6 and Si_2H_6 chemistry [14,18]. The half cycles of Si_2H_6 dosed onto a WF_6 or MoF_6 saturated surface; for the Mo chemistry, the reaction was described as:

$$MoF_5^* + Si_2H_6(g) \rightarrow MoSiH_xF_{3-x}{}^* + SiH_{2-x}F_{2+x}(g) + 2H_2(g) \quad (x = 0, 1 \text{ and } 2)$$

where the asterisks indicate surface species. The authors pointed out that the subsequent WF_6 or MoF_6 doses react with the deposited SiH_xF_y species to form W or Mo metal again.

The reaction of MoF_6 and Si_2H_6 on H-terminated Si demonstrates the potential for $MoSi_x$ ALD on Si-H terminated Si; conversely, for the same series of MoF_6 and Si_2H_6 saturation doses on SiON, no reaction was observed (see Fig. 1(b)). It should be noted that while this sample was nominally SiON, XPS showed only negligible amounts of N on the surface and so this sample is mostly ion damaged SiO_x. After the first 3 pulses of MoF_6, 8% F and negligible Mo (< 1%) were observed. For the rest of the saturation doses, the SiON surface remained unreactive to both MoF_6 and Si_2H_6. This inherent chemical selectivity of SiO_2 (not SiON) was reported earlier using WF_6 and SiH_4 for W metal ALD on Si vs. SiO_2 [13,14,23]. Kalanyan et al. used SiH_4 as a sacrificial reducing agent for W deposition, and the substrate dependent selectivity was explained by the thermodynamically unfavorable reaction between WF_6 and stable Si-O bonds of pristine SiO_2. A similar mechanism is consistent with the selectivity of MoF_6 and Si_2H_6 on Si vs. SiON despite Si_2H_6 being more reactive than SiH_4 and SiON being a less stable film than SiO_2. While the SiON used in this study is ion damaged, the Si is in oxidation states of +3 and +4 and the data is consistent with these strong Si-O, Si-N, SiO-H bonds precluding the Si from forming bonds to Mo (see Fig. S1). DFT models by Kwon et al. show that the stronger SiO-H bond compared to Si-H can raise the activation barrier and enthalpy of reaction for ALD [30].

In Fig. 2, the XPS spectra of Si 2p and Mo 3d for the HF cleaned Si

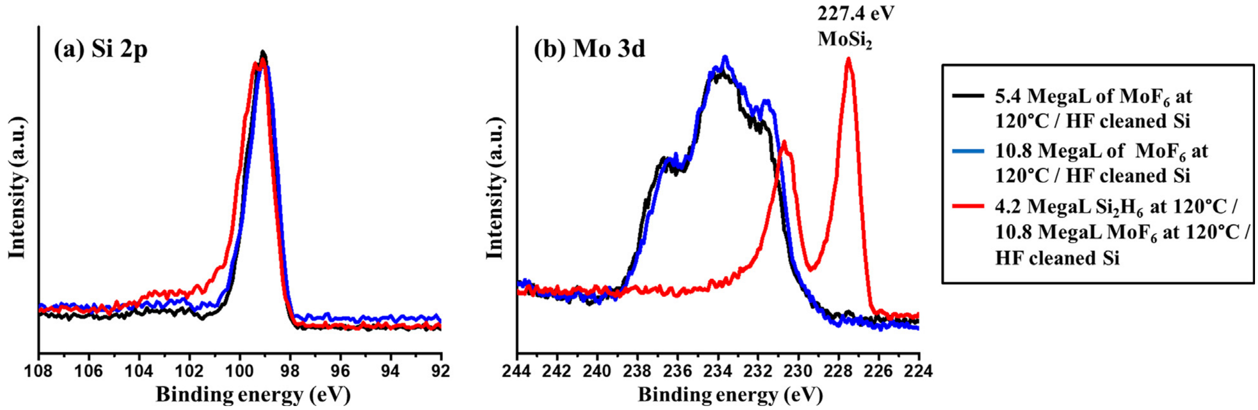

Fig. 2. Oxidation States from XPS peaks of Si 2p and Mo 3d at each experimental step on HF cleaned Si. (a) Si 2p peaks after sequential MoF_6 and S_2H_6 doses shows that Si remained in oxidation state of 0 after the 10.8 MegaL of MoF_6 at 120 °C (blue line) which is consistent with Mo-Si bond formation and no Si-F bonds being present on the surface. After the 4.2 MegaL Si_2H_6 dose at 120 °C (red line), most of the Si stayed in an oxidation state of 0. This is consistent with the formation of a monolayer of $MoSi_2$. A small oxidized Si peak emerged at higher binding energies which might be SiH_xF_{4-x} (x = 2 or 3) or SiO_x at the surface. (b) Mo 3d peaks after sequential MoF_6 and S_2H_6 doses shows that the Mo 3d peaks existed in multiple oxidation states after the saturation dose of MoF_6. (black and blue line) After a Si_2H_6 dose (red line), all of the Mo was reduced and the peak was centered at 227.4 eV which is consistent with $MoSi_2$ formation. (For interpretation of the references to colour in this figure legend, the reader is referred to the web version of this article.)

sample are shown to compare the oxidation states at each experimental step. After the first 5.4 MegaL of MoF_6, the Si 2p peak remained at an oxidation state of 0 which is consistent with Si-Mo bond formation. The Mo 3d peaks appeared at multiple oxidation states which indicates that the surface species are MoF_x with x = 4, 5 and 6 (black line). The additional 5.4 MegaL of MoF_6 did not change the oxidation states of the Si 2p or the Mo 3d peaks (blue line). These results are consistent with the formation of Si-Mo-F_x at the surface. It is noted that the F/Mo ratio was 2.6 after the MoF_6 saturation dose from XPS. (Fig. 1(a)) while the Mo is in oxidation states of 4–6; therefore, it is possible that there is some Mo-O bond formation. A small shoulder peak at a higher binding energy (103 eV) on the Si 2p XPS peak appeared after a 4.2 MegaL of Si_2H_6 dose (red line). This is consistent with Si-F or Si-O formation. The Mo 3d spectra shows that after a single Si_2H_6 dose, all of the Mo is reduced to Mo^0 with a binding energy of 227.4 eV. This is consistent with the formation of a monolayer of $MoSi_x$ and the transfer of any residual oxygen or fluorine from Mo to Si in the form of Si-O and Si-F bonds. A possible simplified reaction of MoF_6 and Si_2H_6 could be described as:

$$MoF_6(g) + 1.5Si_2H_6(g) \rightarrow MoSi_2(s) + SiF_4(g) + 3.5H_2(g) + 2HF(g)$$

ALD characteristics of $MoSi_x$ on the Si substrate and the inherent selectivity over the SiO_2 and SiN_x substrates were verified via XPS of $MoSi_x$ deposition on a patterned sample. Fig. 3 shows the chemical composition of a set of three samples: HF cleaned Si, HF cleaned SiO_2 and HF cleaned patterned sample (note: the raw XPS spectra are presented in Fig. S3). The three samples were loaded together on a single sample holder to ensure that they were exposed to identical deposition conditions. The Si and SiO_2 samples allowed verification of selectivity during deposition on the patterned sample. The patterned sample had SiO_2 layers sandwiched by SiN_x on top of the Si substrate as shown in Fig. 3(d). It is noted that the SiN_x on the patterned sample was actually SiON since it was ion damaged and ashed in O_2 during fabrication. As shown in Fig. 3(a), a 30 s HF clean removed the native oxide on Si. The thermally grown SiO_2 was 300 nm thick and so the 30 s of HF clean did not change the elemental composition or oxidation states of SiO_2. The HF cleaned patterned sample showed a mixture of SiN_x, SiO_x and Si^0. Even though there were Si and SiO_2 samples loaded together to monitor the selectivity of the patterned sample, the blanket films might not be the same as 3D nanostructure features due to the high aspect ratio as well as damage from the patterning processes. Employing a patterned sample in XPS allowed selectivity determination on the nanoscale on realistic surface because the Si^0 component could be distinguished from SiO_2 or SiN_x from XPS. If $MoSi_x$ was deposited selectively on the patterned sample, it was expected that only the attenuation of this Si^0 component from the mixture of SiO_2 and SiN_x would be observed (see Fig. S3).

XPS was performed after 5 ALD cycles of MoF_6 and Si_2H_6 at 120 °C as shown in Fig. 3(b). XPS showed a surface composition of 32% Mo and 10% Si with 39% F on the Si sample which shows a MoF_x rich surface. This is in contrast to a surface closer to $MoSi_2$ after the first ALD cycles. Even though a monolayer of $MoSi_2$ was able to be deposited on Si in the ALD saturation experiments described in Figs. 1 and 2, consecutive ALD cycles did not produce stoichiometric $MoSi_2$. The formation of Si deficient $MoSi_x$ could be due to the surface SiH_xF_y species desorbing during the fluorosilane elimination process and due to residual Mo-F bonds which are not readily removed by standard Si_2H_6 dosing [18,20,22]. For the first 1–3 monolayers, there is an excess of Si from the substrate present to assist in fluorine desorption in the form of SiH_xF_y or SiF_4, but for thicker films, Mo-F surface bonds may persist since the only available Si is from the gaseous Si_2H_6. The overall fluorosilane elimination chemistry using MoF_6 and Si_2H_6 is consistent with one of two chemical reactions:

$$MoF_6(g) + Si_2H_6(g) \rightarrow Mo(s) + 2SiHF_3(g) + 2H_2(g)$$

or

$$2MoF_6(g) + 1.5Si_2H_6(g) \rightarrow 2Mo(s) + 2SiF_4(g) + SiHF_3(g) + 3.5H_2(g) + 2HF(g)$$

It is noted these processes are limited to the first 1–3 monolayers, since cross sectional TEM studies of the patterned sample shows Si substrate depletion of about 1 nm. For the ALD cycles remote from the surface, the depth profile studies below show that the MoF_x is just a surface layer and not a bulk film. There was no $MoSi_x$ deposition on the SiO_2 substrate consistent with highly selective ALD. On the patterned

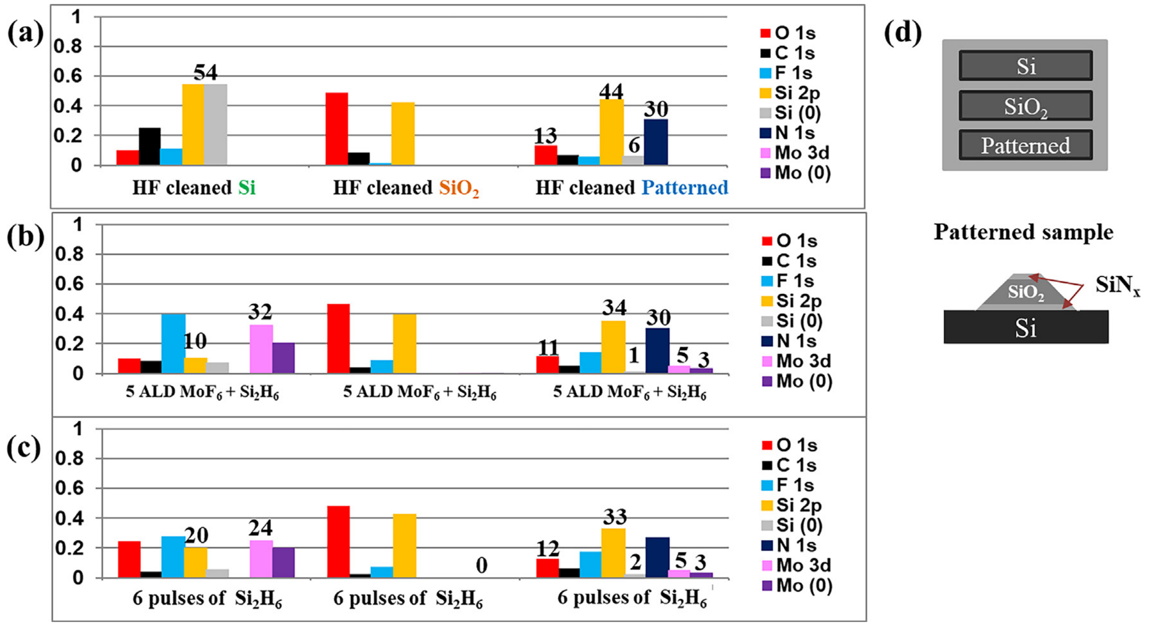

Fig. 3. XPS chemical composition of Si, SiO_2 and a patterned sample after 5 ALD cycles of $MoSi_x$ and subsequent further Si_2H_6 dosing. (a) Chemical composition of HF cleaned Si, SiO_2 and patterned sample. (b) 5 ALD cycles of MoF_6 and Si_2H_6 at 120 °C selectively deposited Si-deficient $MoSi_x$ on Si and not on SiO_2. The Si^0 component of the patterned sample was also selectively attenuated by the $MoSi_x$ deposition. (c) After an additional 25.2 MegaL (6 pulses) of Si_2H_6, more Si was incorporated onto the $MoSi_x$ surface. Selectivity with respect to SiO_2 was maintained during the additional Si_2H_6 pulses. (SiO_2 had 0% Mo and 0% Si^0 throughout the ALD process). (d) A schematic of HF cleaned Si, SiO_2 and patterned samples loaded together on a single sample holder along with a diagram of a patterned sample showing its features.

sample, XPS showed that 5% Mo was deposited, and the Si^0 was attenuated to 1% (The raw XPS peaks are shown in Fig. S3(c)). The fraction of N and O at the surface did not change significantly during ALD on the pattern sample. The data is consistent with Si-deficient $MoSi_x$ being deposited selectivity on the 6% of Si^0 (The grey bar in Fig. 3(a)) on the patterned sample. This selectivity on the pattern samples is consistent with three aspects of the XPS study: (1) There was $MoSi_x$ deposition on the Si sample but not on the SiO_2 sample. (2) After the $MoSi_x$ deposition, only the Si^0 (not the higher oxidation state Si peaks from Si-N and Si-O) was attenuated on the pattered sample. (3) Numerically, ~4% Mo deposition on the patterned sample with 6% Si^0 is proportional to having 32% Mo on the Si sample with 54% Si^0 on the HF clean surface.

To form $MoSi_2$, the three samples were exposed to an additional 25.2 MegaL (6 pulses) of Si_2H_6 at 120 °C (Fig. 3(c)). After the extra Si_2H_6, Si increased to 20% on the Si substrate consistent with Si being incorporated into the film or on the surface. These extra Si_2H_6 doses did not decrease the selectivity for deposition on Si versus SiO_2.

The substrate selectivity of the $MoSi_x$ deposition with respect to SiON along with the effect of post deposition anneal on film composition were investigated. It should be noted that this SiON is actually Si_3N_4 which has been ashed with an O_2 plasma and so this models patterned sample sidewalls after RIE etching. The SiON was loaded into the chamber along with Si and SiO_2 for calibration. Fig. 4(a) shows that the SiON surface is composed primarily of SiN_x after the HF clean. After the 5 cycles of $MoSi_x$ ALD followed by an additional 25.2 MegaL of Si_2H_6, there was 24% Mo and 18% Si on HF cleaned Si while less than 1% Mo was detected on the SiO_x and SiN_x surfaces as shown in Fig. 4(b) (Note, the raw XPS spectra are presented in the supplement). Subsequently, the three samples were annealed at 520 °C for 3 mins which decreased F from 25% to 3% on the Si substrate. The 520 °C PDA also reduced all of the Mo to Mo^0 on the Si substrate and decreased the Si/Mo ratio from 0.75 to ~0.5 at the surface. This is consistent with the desorption of surface F in the form of $SiHF_3$ or SiF_4. The XPS analysis of the high temperature anneal indicates that the F could be removed from the film by the post anneal which may be needed for practical application in MOSFETs [25–27].

Using an in-situ STM and ex-situ AFM, the surface topographies were investigated after the deposition and the high temperature anneal on the Si and SiO_2 samples. A separate sample of HF cleaned Si after 20 cycles of MoF_6 and Si_2H_6 was prepared for the in-situ STM. Fig. 5(a) shows the STM image of $MoSi_x$/HF cleaned Si sample. The $MoSi_x$ film was atomically flat and conformal with an RMS roughness of 2.8 Å. This sample was annealed in-situ at 500 °C for 3 mins in the ultra-high vacuum chamber at a pressure of $\sim 5.0 \times 10^{-10}$ Torr. After the 500 °C anneal, the film became flatter with an RMS roughness of 1.7 Å shown in Fig. 5(b). There was no agglomeration at the surface. Another sample of $MoSi_x$/HF cleaned Si after 5 ALD cycles at 120 °C followed by an in-situ 550 °C anneal was taken into an ex-situ furnace for a 900 °C spike anneal in 5% H_2 balanced with N_2. After the 900 °C spike anneal, AFM was used to obtain the surface morphology. The film retained a sub-nanoscale RMS roughness of 4.75 Å demonstrating that the $MoSi_x$ film has very good thermal stability up to 900 °C (see Fig. 5(c)).

Fig. 5(d) shows an ex-situ AFM image of the SiO_2 surface after dosing 5 ALD cycles at 120 °C followed by an in-situ 550 °C anneal for 3 min in order to confirm the selectivity by counting the number of nuclei on the surface. The density of nuclei was 9 nuclei/μm^2 which confirms the very good selectivity over SiO_2. Lemaire et al. [13] studied the relationship between inherent substrate selectivity and hydroxyl density during tungsten (W) ALD using WF_6 and SiH_4. They reported that an increase in the surface OH density on SiO_2 provokes earlier nucleation of W on SiO_2 (selectivity loss) via a reaction of W-ALD reactants with the surface hydroxyls. The authors also stated that pre-dosing the Si-OH terminated SiO_2 with SiH_4 induces earlier W nucleation by forming a Si monolayer on SiO_2. In present study, Si_2H_6 was employed which is more reactive than SiH_4 due to the weak Si-Si bond; therefore it is likely that Si_2H_6 will react with Si-OH sites on SiO_2 above a threshold exposure. To estimate the selectivity of $MoSi_x$ deposition between H-terminated Si versus OH terminated SiO_2, the surface OH density of the thermally grown SiO_2 was assumed to be ~2 OH/nm^2 as reported by Mueller et al. [29] Assuming $MoSi_x$ deposition on H-terminated Si was 100%, there were only ~10 nuclei/μm^2 out of $\sim 2 \times 10^6$/μm^2 (2 OH/nm^2) hydroxyls on SiO_2 which is consistent with more than 10^6 selectivity between Si-H groups and hydroxyls on SiO_2. Parson et al. [14] reported for the ALD of W using WF_6 and S_iH_4, ~450 nuclei/μm^2 after 30 cycles of W ALD which is about 50× greater than in the present study. There is a previous report of similar selectivity for any selective ALD or CVD process. Chang et al. [24]

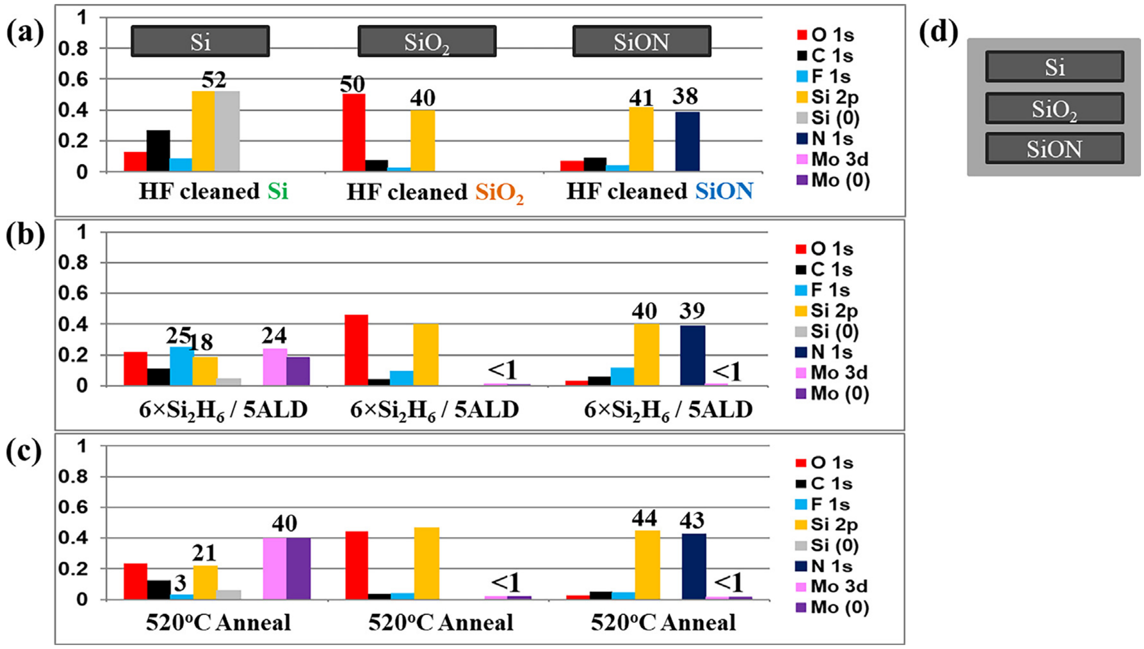

Fig. 4. XPS chemical composition of selective $MoSi_x$ deposition on HF cleaned Si vs SiO_2 and SiON with 520 °C PDA for 3 mins. (a) Chemical composition of Si, SiO_2 and SiON after the HF clean. (b) $MoSi_x$ was selectively deposited only on Si after the 5 ALD cycles of $MoSi_x$ followed by the additional 6 pulses (25.2 MegaL) of Si_2H_6 at 120 °C. (c) Post-deposition anneal was performed at 520 °C for 3 mins. The PDA removed F from the $MoSi_x$ film and reduced all of the Mo to Mo^0. (d) A schematic of HF cleaned Si, SiO_2 and SiON samples loaded together on a single sample holder.

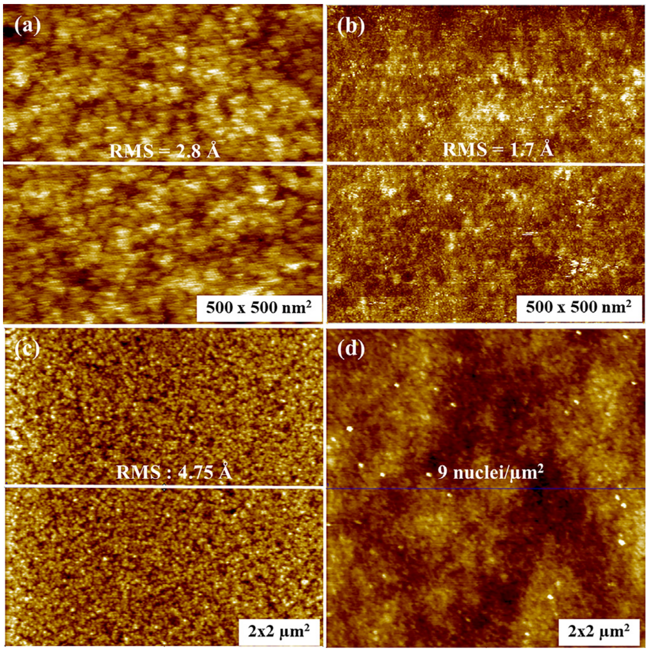

Fig. 5. Surface morphology of Si samples after each stage of ALD and PDA and SiO_2 sample after ALD and PDA. (a) After 20 ALD cycles of $MoSi_x$ on HF cleaned Si, STM shows an atomically flat and conformal surface with an RMS roughness of 2.8 Å. (b) After the PDA at 500 °C for 3 mins, the film got smoother and the RMS roughness decreased to 1.7 Å. (c) 5 cycles of $MoSi_x$ ALD on HF cleaned Si was subjected to the in-situ 550 °C anneal followed by an ex-situ spike anneal at 900 °C. The film did not show agglomeration, and the RMS roughness was 4.75 Å which demonstrates the thermal stability of the $MoSi_x$ film. (d) AFM image of SiO_2 showed only a few $MoSi_x$ nuclei on the surface after the 5 cycles of MoF_6 and Si_2H_6 at 120 °C followed by the 550 °C anneal for 3 mins which is consistent with the high selectivity.

studied the CVD of W by a mixture $WF_6 + H_2 + SiH_4$ and measured the W particles on SiO_2; while they observed a low particle density (20 particles/cm^2), the particles were ~2 μm^2 in size and therefore at least 10^3 larger is mass than the particles in the present study (~1.4×10^{-3} μm^2 in size with ~2 nm height). The high selectivity in the present study is consistent with careful control of wall temperature and using short high pressure Si_2H_6 pulses and longer purge cycles to avoid CVD.

A depth profile study was performed to determine the internal composition of the $MoSi_x$ film. Fig. 6(a) shows XPS of $MoSi_x$/HF cleaned Si after sequential sputtering experiments (Addition raw XPS spectra are presented in the supplement). The $MoSi_x$ film was deposited on HF cleaned Si at 120 °C using 5 ALD cycles of MoF_6 and Si_2H_6 without additional Si_2H_6 incorporation. As the sputtering time increased, the $MoSi_x$ film became thinner until the underlying Si substrate was exposed. The first 10 mins of sputtering decreased the F from 35% to 8% while the Mo shifted from a mixture of oxidized Mo and Mo^0 to pure Mo^0. The data is consistent with the surface F being bonded primarily to Mo. Following consecutive sputtering cycles, the amount of Si increased and the amount of Mo decreased. Furthermore, the amount of Si^0 (gray bars) increased together with the total Si (yellow bar) and reached a maximum at 43% after 100 mins of a total sputtering time. The Si^0 to Mo^0 ratio was employed to distinguish the pure $MoSi_x$ phase because as shown by Wagner et al. as well as Brainard and Wheeler in the pure $MoSi_x$ phase, both Mo and Si are bonded to each other and have an oxidation state of 0 consistent with minimal charge transfer between Mo and Si in the silicide [32,33]. After removal of the silicon oxide and MoF_x species at the surface, the percentage of Si^0 exceeded that of Mo^0. The Si^0:Mo^0 ratio in the bulk of the $MoSi_x$ film was 1.41 which corresponds to a Si-deficient $MoSi_x$ film. It is noted that in the center of the film the Si/Mo ratio is 1.77 therefore, in the absence of background O_2/H_2O, it is possible the Si^0:Mo^0 ratio would be closer to 2.

Fig. 6(b) shows the raw XPS spectra of Si 2p corresponding to each XPS measurement in Fig. 6(a). The Si peak at 99.2 eV increased and broadened to higher binding energy after the 4th sputtering cycle. In contrast, the energy of the of Mo peak corresponded to Mo^0 after each sputtering cycle (Fig. S2). The data is consistent with the bulk $MoSi_x$ film being mostly Si^0 and Mo^0 in the form of $MoSi_x$ while the top surface and the bottom interface was rich in SiO_x. The top SiO_x is consistent with contamination from the chamber environment while the bottom interfacial oxide is consistent with the imperfect ex-situ HF clean. The sub-stoichiometric oxide at the bottom interface did not affect the

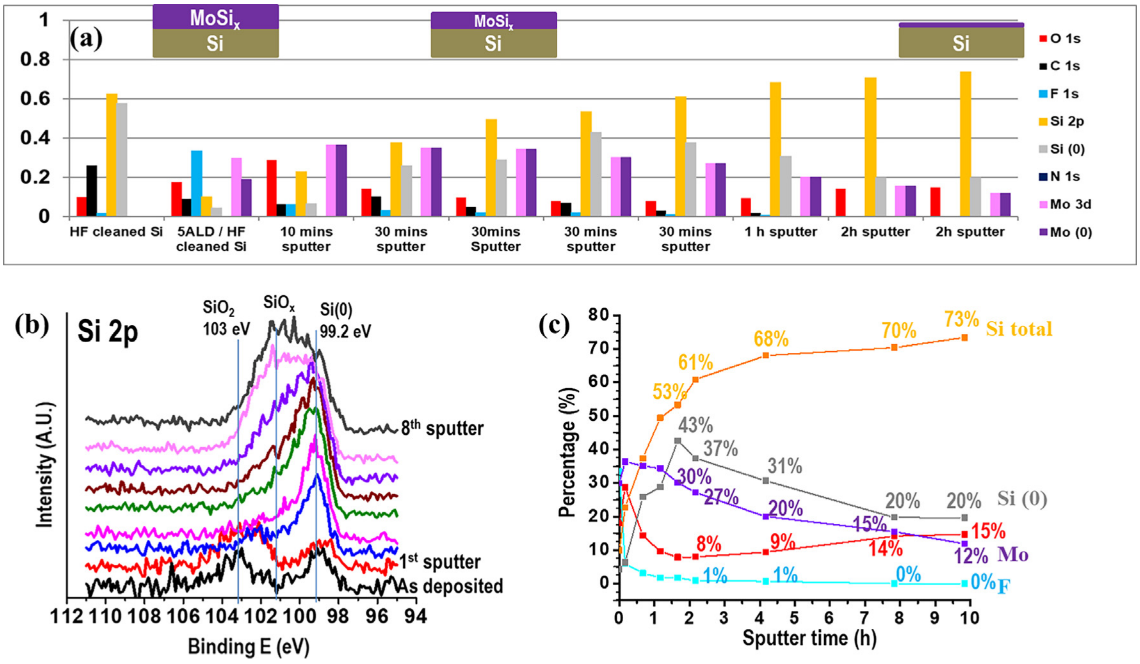

Fig. 6. Depth profiling XPS study of the $MoSi_x$ film. (a) A series of Ar^+ sputtering experiments were performed in conjunction with XPS on HF cleaned Si after the 5 cycles of MoF_6 and Si_2H_6 at 120 °C. (b) XPS peaks of Si 2p after sequential Ar^+ sputtering shows that the bulk of the $MoSi_x$ film consisted mostly of Si^0. (c) The chemical composition of the film is plotted versus Ar^+ sputter time on Si after 5 cycles of MoF_6 and Si_2H_6 at 120 °C. A lens voltage of 5 kV with a beam current of 1.2 μA at 6.0×10^{-7} Torr of Ar was employed.

deposition and film quality indicating that the inherent selectivity of the $MoSi_x$ ALD is sensitive to the quality of the SiO_2. Fig. 6(c) shows the percentages of the chemical components obtained from the XPS measurement in Fig. 6(a). After the 2nd sputtering cycle (40 mins of total sputtering time), F decreased to below 3% and eventually reached 0%. O in the bulk of the film was < 10% but slowly increased to 15% at the $MoSi_x$-Si interface which is consistent with the existence of an interfacial oxide layer.

To understand the effect of the additional Si_2H_6 doses on the Si/Mo ratio of $MoSi_x$ film, XPS depth profiling was performed on a $MoSi_x$ film which had the additional Si incorporation. An additional 6 pulses (25.2 MegaL) of Si_2H_6 were dosed at the end of the 5 ALD cycles of MoF_6 and Si_2H_6 at 120 °C followed by an anneal at 530 °C for 3 mins on dry cleaned Si. This dry clean process uses a downstream plasma of NF_3 and NH_3 with Ar as a carrier gas [31]. Fig. 7(a) presents a series of depth-profile XPS after each experimental step. After the 6 × Si_2H_6/5ALD cycles, there were 28% F, 20% Si, and 28% Mo at the surface. F on the surface was mostly removed after the 530 °C anneal and the Mo was all reduced to Mo^0 which was consistent with the desorption of F in the form of SiH_xF_y or SiF_4 from the surface as presented in Fig. 4(c). The Si/Mo ratio was 0.89 at this step. In comparison, the Si/Mo ratio of the $MoSi_x$ film without the extra Si_2H_6 doses was only 0.33 (see Fig. 7(b)). After removing the surface oxide contamination, the Si^0/Mo^0 in the bulk was 1.32 (Si/Mo = 1.96) for $MoSi_x$ with extra Si_2H_6 pulses. This was comparable to the Si^0/Mo^0 = 1.41 (Si/Mo = 1.77) in the bulk of $MoSi_x$ without extra Si_2H_6 incorporation as depicted in Fig. 7(c). The ratio of Si^0/Mo^0 indicates the stoichiometry of the pure $MoSi_x$ component. This is important for the electrical properties as contact materials in MOSFETs. In this context, the notation of Si^0/Mo^0 indicates the ratio between Si and Mo at oxidation states of 0; conversely, Si/Mo indicates the ratio of the total amount of Si to total amount of Mo in the film including Si and Mo atoms boned to F and O and therefore having higher oxidation states. These results are consistent with the extra Si_2H_6 pulses increasing the Si content at the Si-deficient $MoSi_x$ surface after the ALD cycles. In contrast, the Si/Mo ratios in the bulk of the $MoSi_x$ films were close to stoichiometric $MoSi_2$. Fig. 7(d) shows the XPS percentage of each chemical component in the function of the Ar^+ sputter time which is consistent with the $MoSi_x$ formation in bulk of the film.

Previous studies reported Si_2H_6 and SiH_4 to be sacrificial reactants to reduce metal fluorides for pure metal deposition [14,18,20,22,28]. Seghete et al. previously reported Mo metal deposition on Al_2O_3 using MoF_6 and Si_2H_6 at 130 °C with almost complete removal of Si from the Mo metal film as determined by Auger Electron Spectroscopy (AES) [18]. Even though identical reactants were used at a very similar temperature, there was a significant difference in the Si_2H_6 dosing conditions. For pure Mo metal deposition with minimal Si impurities, 1.5 MegaL of Si_2H_6 was introduced into a high vacuum reaction chamber for 60 s at a constant pressure of 25 mTorr using a leak valve. In the present study, 4.2 MegaL of Si_2H_6 was introduced within 6 s using a pneumatic valve. This is about 3 times larger Si_2H_6 exposure within 10 times shorter dosing time thus a 30× higher partial pressure during the ALD dose. The 30× higher instantaneous pressure during dosing may allow a precursor mediated Si_2H_6 chemisorption layer to remain on the surface long enough to react with the Mo to incorporate more Si into the film. This self-limiting Si CVD component can also explain the larger growth rate of $MoSi_x$ (1.2 nm/cycle) in the present study versus that of pure Mo metal (0.6–0.7 nm/cycle) at a similar process temperature. However, the possibility of the thermal decomposition of Si_2H_6 during the ALD cycles were excluded since the thermal decomposition of Si_2H_6 did not occur below 360 °C (see Fig. S6). It is noted that an alternative explanation is provided by Seghete et al. [18] which is the reaction is sufficiently exothermic that the high pressure

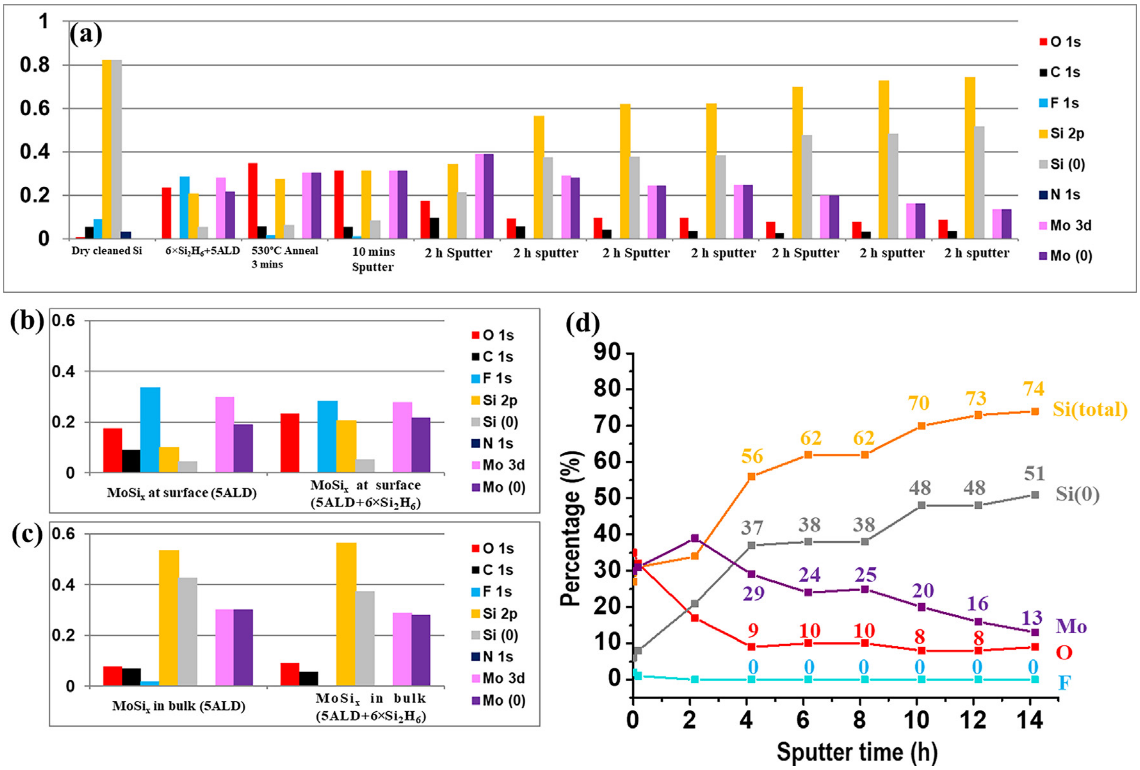

Fig. 7. Depth profiling XPS study of the $MoSi_x$ film with extra Si_2H_6 doses. (a) A series of Ar^+ sputtering experiments were performed in conjunction with XPS on dry cleaned Si after 5 cycles of MoF_6 and Si_2H_6 followed by additional 6 pulses (25.2 MegaL) of Si_2H_6 at 120 °C. (b) Surface composition after 5 ALD cycles of MoF_6 and Si_2H_6 with and without extra Si_2H_6 pulses is compared. Si/Mo ratios were 0.33 for 5 ALD and 0.89 for 5ALD + 6 × Si_2H_6 which is consistent with Si incorporation on the surface. (c) Bulk composition of $MoSi_x$ with and without extra Si_2H_6 pulses is compared after getting rid of the surface contaminations using Ar^+ sputter. Si/Mo ratios were 1.77 for 5 ALD and 1.96 for 5ALD + 6 × Si_2H_6. (d) The chemical composition of the film is plotted versus Ar^+ sputter time on Si after 5 cycles of MoF_6 and Si_2H_6 followed by additional Si_2H_6 pulses at 120 °C. A lens voltage of 5 kV with a beam current of 1.2 μA at 6.0 × 10^{-7} Torr of Ar was employed.

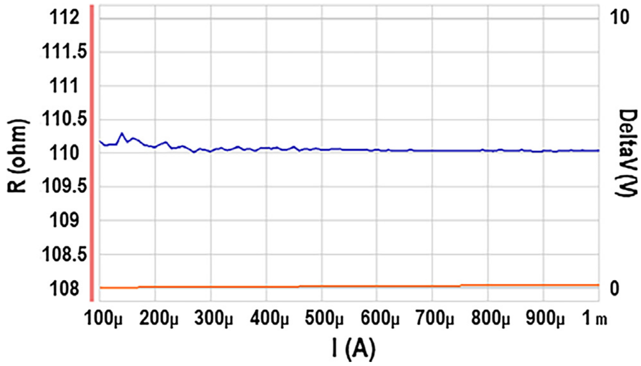

Fig. 8. 4-probe measurement after Ni deposition on the 900 °C annealed $MoSi_x$/Si. Using an infinite sheet model approximation, the resistivity of the $MoSi_x$ film is estimated to be 498 μΩ cm.

Si_2H_6 dosing raises the surface temperature during reaction.

The resistance of the $MoSi_x$ film was measured using a 4-point probe measurement. For the electrical measurement, updoped Si (0 0 1) with > 10,000 Ohm-cm resistance was used as a substrate. For the electrical measurement, 10 cycles of $MoSi_x$ ALD at 120 °C was deposited on an HF cleaned intrinsic (semi-insulating) Si sample followed by an in-situ 550 °C anneal for 3 min and a 900 °C spike anneal in 5% H_2 balanced in N_2. Ni dots were deposited as a probe contact. Fig. 8 shows the resistance of the film versus the current. The resistance was 110 Ohm and, using an infinite sheet approximation, the resistivity could be calculated as:

$$\rho = ktR_{max} = (4.53) \times (10 \times 10^{-7}) \times (110) = 498\ \mu\Omega\ \mathrm{cm}$$

where k is a constant, t is thickness and Rmax is the measured maximum resistance.

A cross-sectional TEM study was performed on the patterned sample to confirm the selectivity of $MoSi_x$ on the nanostructured pattern. On the HF cleaned patterned sample, 5 cycles of $MoSi_x$ ALD followed by an additional 25.2 MegaL of Si_2H_6 were dosed at 120 °C. The elemental composition of this sample at each deposition step is shown in Fig. 3(a–c). Fig. 9(a–b) presents the cross-sectional TEM images of the patterned sample before and after $MoSi_x$ deposition. The TEM image shows complete selectivity of $MoSi_x$ deposition only on Si but not on SiN_x nor SiO_2 without damaging Si substrate by etching (see Fig. 9(c–d)). The thickness of the $MoSi_x$ film deposited on Si was ~6.3 nm after the 5 ALD cycles followed by an additional 25.2 MegaL which gives a growth rate of 1.2 nm/cycle. This higher than expected growth rate was observed by Seghete et al. [18] and ascribed to extra Mo deposition due to the decomposition of MoF_6 from a highly exothermic reaction between MoF_6 and H-Si species. In addition, a direct reaction between the H-terminated Si substrate and MoF_6 could be also attributed to the high growth rate by consuming Si from the substrate. The reaction between the MoF_6(g) and Si(s) could be:

$$MoF_6(g) + 2Si{-}H(g) \rightarrow Si{-}MoF_2(s) + 2SiHF_3(g) + HF(g)$$

or

$$MoF_6(g) + 2Si(s) \rightarrow Si{-}MoF_2(s) + SiF_4(g),$$

where Si-H(s) indicates H terminated Si surface and Si-MoF_2(s) indicates the MoF_2 surface species bonded to the Si atoms of the surface. However, extra Si_2H_6 pulses of high pressure after 5 cycles may incorporated more Si into the film which is consistent with the high growth rate because the consumption of Si from the surface on patterned samples was very small as shown in Fig. 9. Due to the high growth rate per cycle of $MoSi_x$ ALD, 5 ALD cycles is sufficient for contact materials. There was 2.8 nm of an interface oxide layer between the $MoSi_x$ film and the Si substrate which is consistent with the results in Fig. 6. This could be improved by an in-situ clean such as a plasma clean at the sample preparation step.

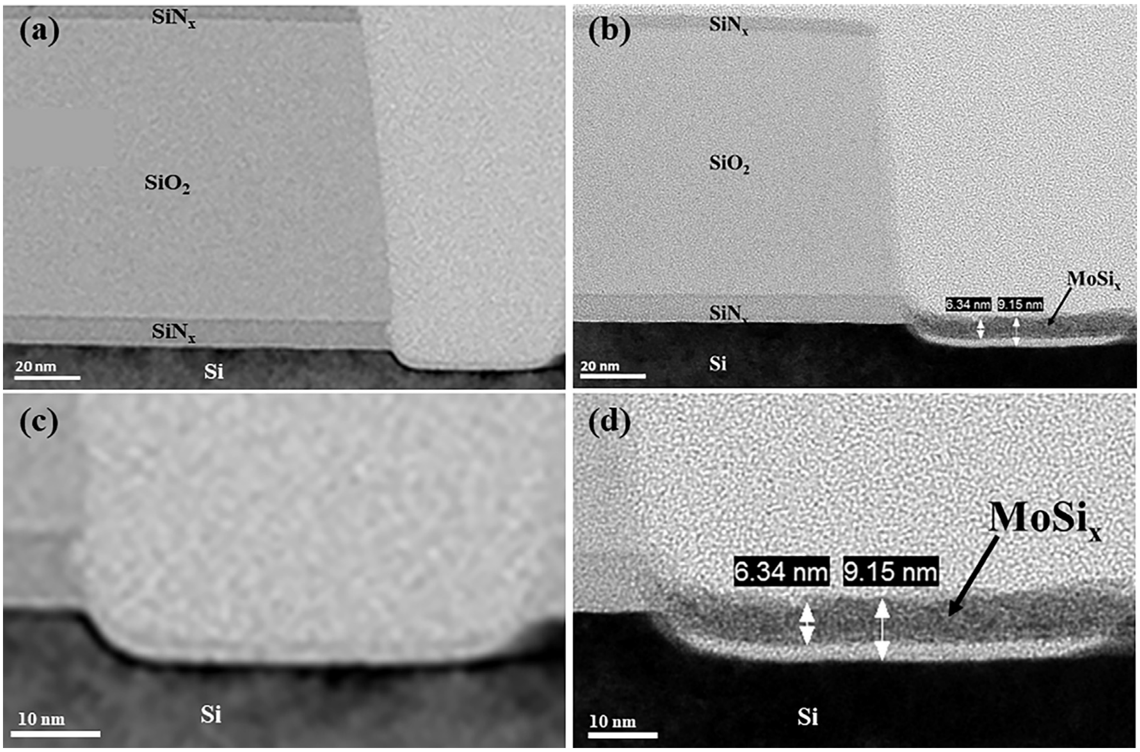

Fig. 9. Selective ALD on a patterned sample. (a) Cross-sectional TEM image of the patterned sample before the deposition. (b) Cross-sectional TEM image of the HF cleaned patterned sample after 5 cycles of MoF_6 and Si_2H_6 at 120 °C with a continuous N_2 purge. 6.34 nm of $MoSi_x$ was selectively deposited only on Si and not on SiO_2 nor SiN_x. (c) Magnified Si region of the patterned sample before the deposition. (d) Magnified Si region of the patterned sample after the $MoSi_x$ deposition shows that $MoSi_x$ was deposited without damaging Si substrate by etching.

4. Conclusion

Selective atomic layer deposition of sub-stoichiometric $MoSi_2$ was achieved by an inherently selective process on hydrogen-terminated Si versus thermally grown SiO_2, ion damaged SiON, and SiN_x. This inherent selectivity is based on the favorable reactivity of MoF_6 and Si_2H_6 on H-Si but not on SiO_2 or SiN_x since Si-O, Si-N, and SiO-H bonds are strong enough that they cannot be cleaved by either precursor at 120 °C. Both MoF_6 and Si_2H_6 showed self-limiting behavior which allowed deposition of a highly conformal and smooth film with a root mean square (RMS) roughness of 2.8 Å. Post-annealing in ultra-high vacuum at 500 °C for 3 min further decreased the RMS roughness to 1.7 Å. The quality of the film was preserved even after a 900 °C spike anneal in an H_2/N_2 environment which is consistent with very good thermal stability. A depth profiling XPS study revealed that the bulk of the $MoSi_x$ film is close to stoichiometric $MoSi_2$ (Si/Mo = 1.7–1.9) with $< 10\%$ oxygen and fluorine. The surface of the $MoSi_x$ film after 5 ALD cycles showed a highly Si-deficient $MoSi_x$ surface with Si/Mo ratio of 0.33, and this Si/Mo ratio at the surface could be improved to 0.89 by pulsing extra Si_2H_6. The selectivity of $MoSi_x$ was examined on nanoscale patterned features of SiO_2 and SiN_x. The cross-sectional TEM imaging shows that the selectivity is retained on the nanoscale and that $MoSi_x$ can be selectively deposited on Si without substrate consumption. A large growth rate of 1.2 nm/cycle allows only 5 ALD cycles to be sufficient for its purpose as a contact material. This inherently selective $MoSi_x$ deposition would obviate the need for lithography on complicated 3D MOSFET structures (FinFETs). The selectivity for Si-H bonds vs SiO-H bonds exceeds 10^6 showing that with careful choice of precursor, extreme selectivity is possible on the nanoscale even without the use additional passivation layers. The study also showed that ALD of silicide versus metal could readily be switched while retaining selectivity by changing the partial pressure during the ALD pulse of the reductant.

Acknowledgements

Funding support from Applied Materials is gratefully acknowledged. The electrical measurements were facilitated by the San Diego Nanotechnology Infrastructure (SDNI) which is supported by the National Science Foundation (NSF) to Nano3 (Grant ECCS-1542148).

Appendix A. Supplementary material

Supplementary data associated with this article can be found, in the online version, at https://10.1016/j.apsusc.2018.08.072.

References

[1] K. Lee, S.W. Park, M.J. Ko, K. Kim, N.-G. Park, Selective positioning of organic dyes in a mesoporous inorganic oxide film, Nat. Mater. 8 (2009) 665–671.

[2] J. Xie, X. Yang, B. Han, Y. Shao-Horn, D. Wang, Site-selective deposition of twinned platinum nanoparticles on $TiSi_2$ nanonets by atomic layer deposition and their oxygen reduction activities, ACS Nano 7 (2013) 6557–6345.

[3] W.-H. Kim, F.S.M. Hashemi, A.J.M. Mackus, J. Singh, Y. Kim, D. Bobb-Semple, Y. Fan, T. Kaufman-Osborn, L. Godet, S.F. Bent, A process for topographically selective deposition on 3D nanostructures by ion implantation, ACS Nano 10 (2016) 4451–4458.

[4] J.A. Liddle, G.M. Gallatin, Nanomanufacturing: a perspective, ACS Nano 10 (2016) 2995–3014.

[5] D.G. Lishan, H.F. Wong, D.L. Green, E.L. Hu, J.L. Merz, D. Kirillov, Dry etch induced damage in GaAs investigated using Raman scattering spectroscopy, J. Vac. Sci. Technol., B: Microelectron. Process. Phenom. 7 (1989) 556–560.

[6] C.H. Jan, U. Bhattacharya, R. Brain, S.J. Choi, G. Curello, G. Gupta, W. Hafez, M. Jang, M. Kang, K. Komeyli, T. Leo, N. Nidhi, L. Pan, J. Park, K. Phoa, A. Rahman, C. Staus, H. Tashiro, C. Tsai, P. Vandervoorn, L. Yang, J.Y. Yeh, P. Bai, A 22nm SoC platform technology featuring 3-D tri-gate and high-k/metal gate, optimized for ultra low power, high performance and high density SoC applications, in: IEEE Int. Electron Devices Meet., 2012, pp. 3.1.1–3.1.4.

[7] M. Fang, J.C. Ho, Area-selective atomic layer deposition: conformal coating, subnanometer thickness control, and smart positioning, ACS Nano 9 (2015) 8651–8654.

[8] M.H. Park, Y.J. Jang, H.M. Sung-Suh, M.M. Sung, Selective atomic layer deposition of titanium oxide on patterned self-assembled monolayers formed by microcontact printing, Langmuir 20 (2004) 2257–2260.

[9] A. Mameli, M.J.M. Merkx, B. Karasulu, F. Roozeboom, W.M.M. Kessels, A.J.M. Mackus, Area-selective atomic layer deposition of SiO_2 using acetylacetone as a chemoselective inhibitor in an ABC-type cycle, ACS Nano 11 (2017) 9303–9311.

[10] F.S. Minaye Hashemi, C. Prasittichai, S.F. Bent, Self-correcting process for high quality patterning by atomic layer deposition, ACS Nano 9 (2015) 8710–8717.

[11] S.E. Atanasov, B. Kalanyan, G.N. Parsons, Inherent substrate-dependent growth initiation and selective-area atomic layer deposition of TiO_2 using “water-free” metal-halide/metal alkoxide reactants, J. Vac. Sci. Technol. A 34 (2015) 01A148-1-9.

[12] M.M. Kerrigan, J.P. Klesko, S.M. Rupich, C.L. Dezelah, R.K. Kanjolia, Y.J. Chabal, C.H. Winter, Substrate selectivity in the low temperature atomic layer deposition of cobalt metal films from bis(1,4-di-tert-butyl-1,3-diazadienyl)cobalt and formic acid, J. Chem. Phys. 146 (2017) 052813-1–8.

[13] P.C. Lemaire, M. King, G.N. Parsons, Understanding inherent substrate selectivity during atomic layer deposition: Effect of surface preparation, hydroxyl density, and metal oxide composition on nucleation mechanisms during tungsten ALD, J. Chem. Phys. 146 (2017) 052811-1–9.

[14] B. Kalanyan, P.C. Lemaire, S.E. Atanasov, M.J. Ritz, G.N. Parsons, Using hydrogen to expand the inherent substrate selectivity window during tungsten atomic layer deposition, Chem. Mater. 28 (2016) 117–126.

[15] A.H. Reader, A.H.V. Ommen, P.J.W. Wijs, R.A.M. Wolters, D.J. Oostra, Transition metal silicides in silicon technology, Rep. Prog. Phys. 56 (1992) 1397–1467.

[16] S.P. Murarka, Transition metal silicides, Ann. Rev. Mater. Sci. 13 (1983) 117–137.

[17] M.Y. Tsai, H.H. Chao, L.M. Ephrath, B.L. Crowder, A. Cramer, R.S. Bennett, C.J. Lucchese, M.R. Wordeman, One-micron polycide (WSi_2 on Poly-Si) MOSFET technology, J. Electrochem. Soc. 128 (1981) 2207–2214.

[18] D. Seghete, G.B. Rayner Jr., A.S. Cavanagh, V.R. Anderson, S.M. George, Molybdenum atomic layer deposition using MoF_6 and Si_2H_6 as the reactants, Chem. Mater. 23 (2011) 1668–1678.

[19] K. Bernal-Ramos, M.J. Saly, R.K. Kanjolia, Y.J. Chabal, Atomic layer deposition of cobalt silicide thin films studied by in situ infrared spectroscopy, Chem. Mater. 27 (2015) 4943–4949.

[20] T. Proslier, J.A. Klung, J.W. Elam, H. Claus, N.G. Becker, M.J. Pellin, Atomic layer deposition and superconducting properties of NbSi films, J. Phys. Chem. C 115 (2011) 9477–9485.

[21] Y.J. Chabal, G.S. Higashi, K. Raghavachari, Infrared spectroscopy of Si(111) and Si (100) surfaces after HF treatment: hydrogen termination and surface morphology, J. Vac. Sci. Technol., A 7 (1989) 2104–2019.

[22] J.W. Klaus, S.J. Ferro, S.M. George, Atomic layer deposition of tungsten using sequential surface chemistry with a sacrificial stripping reaction, Thin Solid Films 360 (2000) 145–153.

[23] E.K. Broadbent, C.L. Ramiller, Selective low pressure chemical vapor deposition of tungsten, J. Electrochem. Soc. 131 (1984) 1427–1433.

[24] K.M. Chang, S.W. Wang, C.H. Li, J.Y. Tsai, T.H. Yeh, Reduction of selectivity loss probability on dielectric surface during chemical vapor deposition of tungsten using fluorinated oxide and removing silanol units on dielectric surface, Jpn. J. Appl. Phys. 35 (1996) 6555–6561.

[25] D.-S. Choi, Fluorine effects on NMOS characteristics and DRAM refresh, Semicon. Sci. Technol. 12 (2012) 41–45.

[26] Y. Mitani, H. Satake, Y. Nakasaki, A. Toriumi, Improvement of charge-to-breakdown distribution by fluorine incorporation into thin gate oxides, IEEE Trans. Electron Devices 50 (2003) 2221–2226.

[27] D.-G. Lin, T.A. Rost, H.S. Lee, D.-Y. Lin, A.J. Tsao, B. McKee, The effect of fluorine on MOSFET channel length, IEEE Electron Dev. Lett. 14 (1993) 469–471.

[28] Ph. Gouy-Pailler, Ph. Lami, R. Morales, Selective deposition of tungsten by chemical vapour deposition from SiH_4 reduction of WF_6, Thin Solid Films 241 (1994) 374–377.

[29] R. Mueller, H.K. Kammler, K. Wegner, S.E. Prastsinis, OH surface Density of SiO_2 and TiO_2 by thermogravimetric analysis, Langmuir 19 (2003) 160–165.

[30] J. Kwon, M. Saly, M.D. Halls, R.K. Kanjolia, Y.J. Chabal, Substrate selectivity of $(tBu\text{-}Allyl)Co(CO)_3$ during thermal atomic layer deposition of cobalt, Chem. Mater. 24 (2012) 1025–1030.

[31] C. Ahles, J.Y. Choi, A. Kummel, A dry NF3/NH3 plasma clean for removing Si native oxide and leaving a smooth Si surface, in: Presented at Materials Research Society, Phoenix, the United States, April 6, 2018; EP01.10.04.

[32] C.D. Wagner, D.E. Passoja, H.F. Hillery, T.G. Kinisky, H.A. Six, W.T. Jansen, J.A. Taylor, Auger and photoelectron line energy relationships in aluminum-oxygen and silicon-oxygen compounds, J. Vac. Sci. Technol. 21 (1982) 933–944.

[33] W.A. Brainard, D.R. Wheeler, An XPS study of the adherence of refractory carbide silicide and boride rf-sputtered wear-resistant coatings, J. Vac. Sci. Technol. 15 (1978) 1800–1805.